Resolving Flow Structures Inside Three Dimensional Packed Beds with Gas Flow by Ray Tracing Particle Image Velocimetry

Christin Velten[1,*], Mirko Ebert[2], Christian Lessig[2;3], Katharina Zähringer[1]

1: Lehrstuhl für Strömungsmechanik und Strömungstechnik,
Otto-von-Guericke-Universität Magdeburg, 39106 Magdeburg, Germany
2: Institute for Simulation and Graphics, Department of Computer Science,
Otto-von-Guericke-Universität Magdeburg, 39106 Magdeburg, Germany
3: European Centre for Medium Range Weather Forecasts,
53175 Bonn, Germany
* Correspondent author: christin.velten@ovgu.de

Keywords: PIV, ray tracing, gas flow, spherical packed beds

ABSTRACT

Two different configurations are investigated in this study by ray tracing Particle Image Velocimetry to access the interior of different spherical packing structures. Configuration 1 consists of a regular bidisperse packed bed of 10mm and 40mm spheres based on a body centred cubic arrangement. Ray tracing Particle Image Velocimetry was performed behind two spheres in the 40mm layer for particle Reynolds numbers from 200 to 700. The averaged velocity flow fields show the jet structures according to the pores between the underlying smaller spheres and the influence of the large spheres. Since ray tracing Particle Image Velocimetry is suffering from experimental and numerical limitations, planar 2D Particle Image Velocimetry measurements are performed to obtain spatially highly resolved validation data in the optically accessible void pores. These measurements were performed at different height positions in the bed showcasing that similar flow fields appear in the different pores.

Configuration 2 deals with the jet flow (Re=5900) around an individual sphere, part of a body centred cubic arrangement of d=40mm spheres. The emphasis lays on the temporally resolved snapshot data of the turbulent jet flow obtained by ray tracing Particle Image velocimetry.

Data obtained from both configurations is used for a comprehensive discussion of the chances and challenges of ray tracing Particle Image Velocimetry. Limitations appear on the experimental side like generation of depth of field, illumination and reflections, sufficient measurement signal and accuracy of the geometry, but also on the numerical side like the reproduction of the geometry, material properties and real world conditions. Since all these phenomena are interlinked, performing the ray tracing method in more complex systems is questionable.

1. Introduction

Applying optical measurement techniques, such as Particle Image Velocimetry (PIV), to three dimensional solid-gas systems within a packed bed, is challenging because of the necessity of

optical access. By replacing the packing with transparent material, optical distortions are introduced to the measurement data, leading to erroneous results which do not represent the features of the flow. Common approaches such as refractive index matching e.g. (Nguyen et al., 2019; V. A. Patil & Liburdy, 2013), allow to avoid the distortions, but only with liquids as working fluid.

For gas-solid systems, without post-treatment of the appearing distortions, measurements are limited to regions where direct optical access is available as on the surface of the packed bed or in directly accessible interstices between the particles. In our previous work (Velten & Zähringer, 2023) we investigated by planar 2D PIV the flow inside a packed bed reactor of 21 layers of d=40mm spheres in a body centred cubic (bcc) arrangement at the surface of the bed and in the optically accessible interstices for particle Reynolds numbers from 200 to 500. The data shows that the flow is less stable at the bed surface while in the interior similar and stable flow structures appear at different bed height positions. A reactor of d=25.5mm particles in simple cubic and bcc arrangement was investigated by stereo PIV horizontally above its surface for particle Reynolds numbers up to 400 by S. Patil et al., (2024). The authors state that jets appear above the bed, at the locations of the pores of the packing. Maximum jet velocities were measured close to the centre of the simple cubic arrangement and were shifted to the peripheral pores in the bcc arrangement.

For insights to the flow behind the transparent packing material, different approaches can be considered for distortion treatment. Kováts et al. (2015) used an advanced calibration strategy for hollow sphere particles to correct for distortion and allow for planar 2D PIV in a packed bed with gaseous flow. As an alternative, the image data can be post-treated with a ray tracing (RT) based distortion correction before standard PIV evaluation (Martins et al., 2018a, 2018b). This ray tracing PIV (RT-PIV) is demanding on both, the numerical and experimental point of view (Velten et al., 2024). An extensive calibration procedure which delivers the geometric parameters of the transparent system as well as a standard calibration for PIV are necessary to get the required accuracy of the model geometry.

In the present work, a 3D-printed base packing (12x12 spheres with d=10mm in a bcc arrangement) holds bigger transparent spheres (d=40mm) in the measurement position, and allows for a defined placement of a calibration target and the geometrical position of the packing relative to the PIV-camera. With an additional numerical optimization step, concerning the position and the refractive index of the spheres under consideration, the real world geometry of the setup, which might vary from the ideal one due to manufacturing inaccuracies, can be reproduced in the ray tracing simulation to ensure a high quality correction of the distorted image data. Thus PIV measurements of the gas velocity fields inside the complete packing become possible in this study.

Additionally, particle Reynolds numbers Re_P in the range from 200 to 700 were investigated by standard planar 2D PIV measurements in the optically directly accessible regions of the packing (interstices between the d=40mm spheres) for validation of the RT-PIV measurements. RT-PIV was also used for measurements of the flow field of a turbulent jet (Re=5900) surrounding a sphere assembly. A critical discussion of all these results allows to shed light on the opportunities and bottlenecks of RT-PIV.

2. Experimental setup

The general experimental setup consists of a double-pulse Nd:YAG PIV-laser (Quantel Q-smart Twins 850 and Innolas SpitLight Compact 400) operated at a wavelength of 532nm for creating a laser light sheet. For more detailed information about the laser parameter sduring the different measurement series see Sec. 2.3. An Imager CX 12MP camera from LaVision GmbH equipped with a 50mm camera lens (FL-BC5024-9M from Ricoh Deutschland GmbH) is used for capturing the Mie-scattering of the Di-Ethyl-Hexyl-Sebacat (DEHS) droplets provided by a liquid nebulizer Type AGF 10.0 from Palas GmbH. The airflow is controlled by a Bronkhorst Mass-flow Controller (D-6371; 500 l/min air).
The test rigs, a bidisperse packing (Configuration 1) and a sphere arrangement with a jet surrounding the central sphere (Configuration 2), can be placed on a traversing unit to generate different measurement positions.

2.1 Bidisperse packing (Configuration 1)

3D-printed modules of two layers of 12x12 d=10mm spheres in a bcc arrangement are mainly used (Fig. 1 centre top) in this setup. To ensure the stability of the modules an overlap of the spheres is required which is generated by a small increase of the sphere diameter to d=10.25mm. These modules allow to generate different packing structures by including further d=10mm or 40mm spheres which can be transparent (nBK-7 glass) if optical access is required in the measurement position. The packing investigated in this work is shown in Fig. 1 left as a cut at the main investigation plane and is considered as Configuration 1. In this configuration we use two of the aforementioned modules, an additional layer of d=10mm spheres with 3x3 d=40mm spheres on top. This pattern is repeated two more times and two additional modules are stacked on top. An acrylic box with a height of 380 mm is placed as an outlet zone. The entire bed height is 241.37 mm. The main investigation plane, which is the plane behind two of the d=40mm spheres, was chosen because the recoverable area for RT-PIV is the highest behind even numbers of spheres

(Velten et al., 2024). The top view of the configuration is shown on the lower centre image in Fig. 1. The circles represent the underlying d=40mm spheres with the measurement plane as a green line. The PIV-camera is positioned perpendicular to this line (that would be the bottom of the top view).

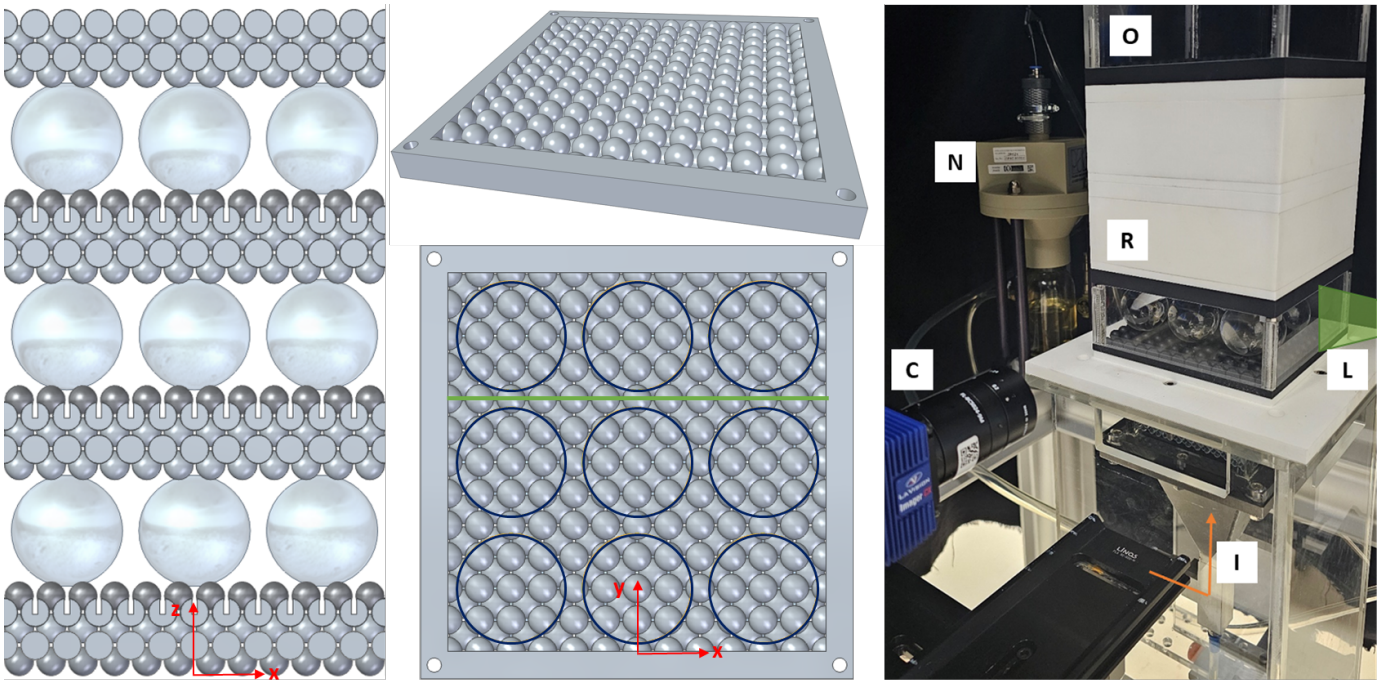

Figure 1 Inner structure of Configuration 1, a bidisperse packing with d=10mm and d=40mm spheres, is shown on the left, as a cut through the main measurement plane behind two of the d=40mm spheres. This is highlighted as a green line in the top view of the configuration (lower centre image). Here the dark circles represent the underlying d=40mm spheres which are not directly visible in the top view. In the centre top image, the basis module is shown which is used to create the packing. The integration of Configuration 1 in the PIV setup is shown in the right image. The bulk reactor including the packing material (R) is placed on the inlet zone (I) which is fixed to a traversing unit and the outlet zone (O) is placed on top. Illumination takes place by the laser light sheet (L) and the signal from the DEHS tracer particles provided by a nebulizer (N) is captured by a camera (C). Note that in the real measurements, contrary to the image, the camera is placed further away to be able to generate the necessary depth of field for performing RT-PIV.

The entire packing is connected to an inlet zone which was used in a previous work (Velten et al., 2024; Velten & Zähringer, 2023) and can be included to the PIV setup as shown in Fig. 1 right. The transparent spheres and acrylic frame are moved to each measurement position as well as black-coloured modules are used above and below the measurement region to reduce reflections. The lower black-coloured module provides a slit where the calibration target can be fixed with connection to the geometry which is crucial for the calibration steps of the RT-PIV evaluation detailed in Sec. 3.

The inlet flow is adjusted to reach the particle Reynolds number Re_P (Eq. 1) defined by the theoretical porosity of a bcc packing of ϕ=0.32 and the diameter of the 40mm spheres, the internal velocity v_{int} and the density ρ and dynamic viscosity μ at ambient conditions (T=20°C; 1bar):

$$Re_P = \frac{v_{int} \cdot \rho \cdot d_P}{\mu} \quad (1)$$

The flow rates for the Re_P used in this study are listed in Table 1.

Table 1: Particle Reynolds numbers and its corresponding flow rates

Re_P [-]	200	300	400	500	700
Q [L/min]	25.45	38.17	50.09	63.62	89.07

2.2 Jet dispersion around a sphere (Configuration 2)

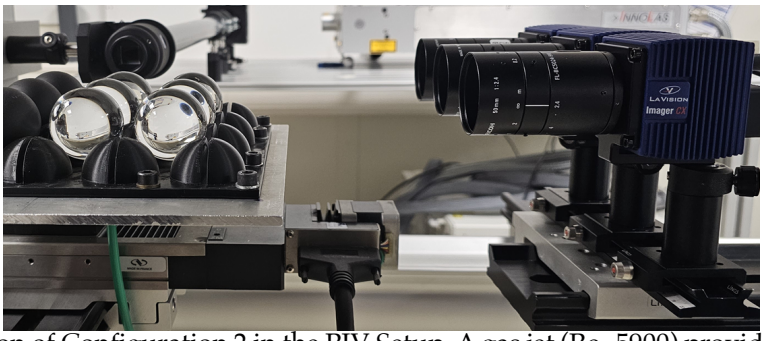

Figure 2 Integration of Configuration 2 in the PIV-Setup. A gas jet (Re=5900) provided by a tube with an inner diameter of d_i=4mm surrounds the central sphere of a two-layer packed bed of d=40mm spheres in bcc arrangement. Note that in the real measurements, contrary to the image, the cameras are placed further away to be able to generate the necessary depth of field for performing RT-PIV. The setup allows to use three cameras for the investigation of different perspectives to the measurement plane. For the data presented in this study, only the central camera is used.

A ground plate with 4x4 half spheres with d=40mm is 3D-printed and allows to hold one layer (3x3) of nBK-7 glass spheres in a bcc arrangement. Each bottom half sphere has a slit in the centre to place a calibration target with connection to the geometry. This is crucial for the calibration steps of the RT-PIV evaluation detailed in Sec. 3. Below the central glass sphere, a pipe with an inner diameter d_i=4mm delivers an airflow surrounding the central sphere.

Here also, the measurement was carried out behind two glass spheres to allow for a maximum reconstructable area. A Reynolds number of approximately Re=5900, based on the diameter of the jet inlet, and corresponding to a volume flow rate of Q = 1 m^3/s was investigated. Fig. 2 shows the test rig installed in the PIV setup. Three cameras are placed allowing for the recording of different perspectives. In the present work only the images of the central camera are used.

2.3 Settings and recording parameters

In Table 2 the different recording and setting parameters are listed for each measurement series. The main difference between the planar 2D PIV and RT-PIV is the depth of field (DoF) necessary for the acquisition of focused measurement images. While in 2D PIV only the plane illuminated by the laser light sheet has to be in focus, which corresponds to a thin required DoF, this plane is shifted during RT-PIV by the lens effect of the transparent spheres in the direction of the camera requiring a highly increased DoF. To fulfil the requirement, the DoF can be increased by placing the camera further away from the plane illuminated by the light sheet and by closing the aperture. The aperture of the chosen lens allows for a continuous adjustment. Both lead to a loss of contrast for the measurement image and less resolution of the final velocity field in comparison to the standard planar 2D PIV method. To provide an idea of this difference, the scaling factor and the distance of the camera from the measurement plane are also listed in Table 2.

Table 2 Overview of important recording and setup parameters for the different measurement configurations

	Position	**Technique**	**Laser Frequency; Laser Energy**	**Re_P [-] (Number of recorded images)**	**Aperture**	**Camera distance**	**Scaling factor [pixel/m]**
Bidisperse packing (1)	inside packing	RT-PIV	Quantel 10Hz; 46mJ/pulse	200 - 700 (1000)	~f12	~ 1042mm	18.92
	between particles	2D PIV	Quantel 10Hz; 10mJ/pulse	200 - 400 - 700 (200 - 500)	f2.8	~ 348mm	58.26/57.02
Jet around spheres (2)	behind central sphere	RT-PIV	Innolas 1Hz; 170mJ/pulse	5900 (100)	~f12	~1200mm	16.3

3. Methods

For the planar 2D PIV, images of a calibration target (Type 058-5 from LaVision) are used to perform a calibration in DaVis 10.2. Afterwards the background and static artefacts caused by reflections are removed by subtracting the siding minimum over 3 images. Image normalisation improves the quality of the particle field images if necessary and a mask is applied to regions without measurement signal. By a multipass cross correlation method with decreasing interrogation window size (256x256 pixel² to 64x64 pixel² for RT-PIV or to 32x32 pixel² for planar 2D PIV) the velocity vector field is calculated and incorrect vectors are filtered.

Post-processing of the RT-PIV data consists of the same processing steps, but includes an additional distortion correction which is carried out together with the calibration by using an in-

house software. The workflow for RT-PIV is shown in Fig. 3. Additional images of a specially designed calibration target, shown in Fig. 4., are necessary. The calibration target is placed with connection to the 3D-printed geometry and is imaged at two different depth positions with and without the transparent packing material. These images ("Target" upper left in Fig. 3) are used to gain the camera calibration parameters but also the exact positioning of our entire system with respect to the camera, which is necessary to perform an accurate ray tracing simulation.

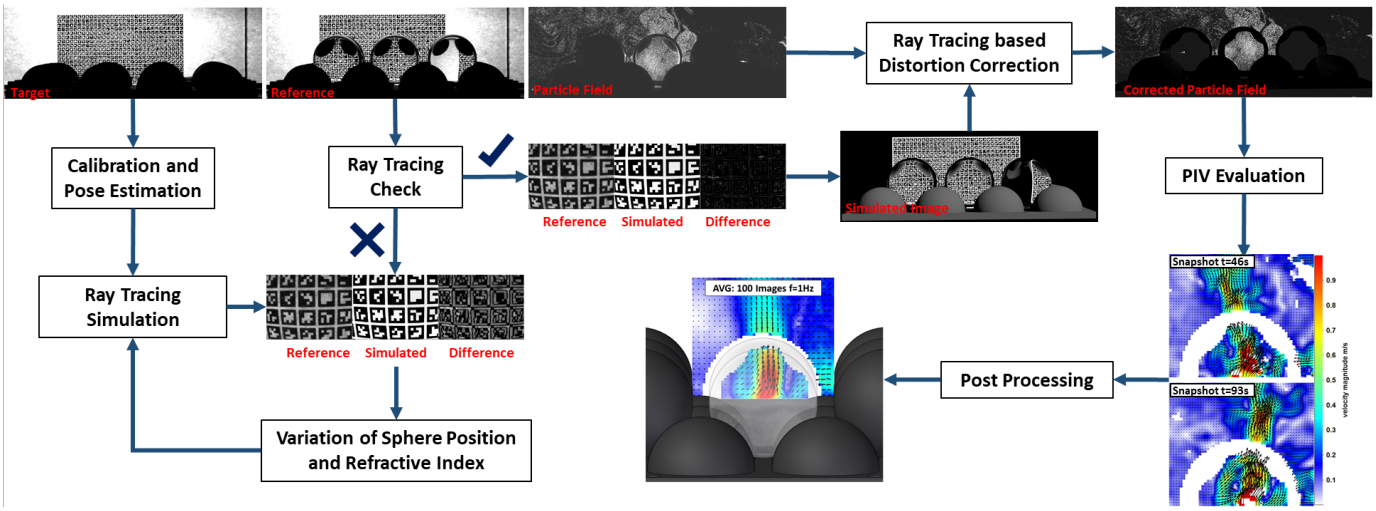

Figure 3 Overview of the RT-PIV workflow exemplarily shown based on configuration 2. From the raw data (calibration and particle field images, top left) to the evaluated vector fields (bottom right) including all necessary processing steps for the distortion correction.

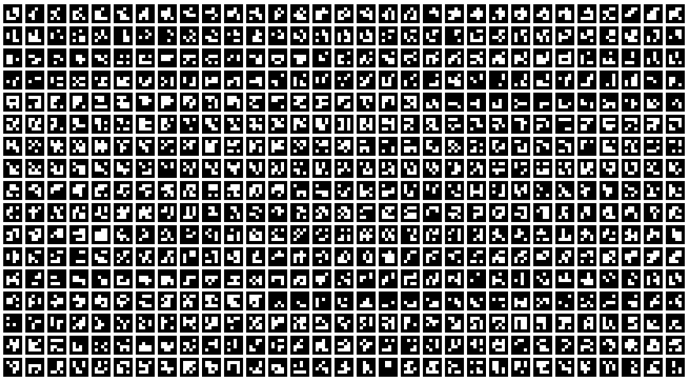

Figure 4 AruCo marker based calibration target for RT-PIV

After determining the camera parameters and the position of the geometry relative to the camera sensor, the experimental scene can be simulated ("Simulated Image" centre right in Fig. 3). By comparing the simulated image of the glass spheres in front of the calibration target with the experimental one ("Reference" top row in Fig. 3) we ensure that the ray tracing correction is carried out properly. Deviations might appear because of differences between the ideal conditions

assumed in the simulation and the real world as e.g. manufacturing tolerances. Therefore, a numerical optimization of the sphere position and refractive index is performed (bottom left in Fig. 3). By varying the parameters in the simulation and comparing the output with the calibration images where the spheres are placed in front of the target, the ideal parameters can be found and ensure a proper distortion correction. After validating that the experimental scene can be reproduced by the simulation, the particle fields can be corrected (top right in Fig. 3). The ray tracing simulation itself is then based on a twostep process. First, the particle field is considered as a light source situated at the measurement plane with the transparent geometry in front of it, where each image position is traced back to the camera sensor representing the distorted light paths. By removing in the second step of the simulation the transparent geometry, the light paths without distortion can be obtained and are traced back to the image plane which allows to correct for the distortions. Then, the PIV evaluation can take place as described before with these corrected images (bottom right in Fig. 3).

4. Results & Discussion

The obtained flow fields for both configurations are presented and discussed in this section. While for Configuration 1 the emphasis lays on averaged flow field data, Configuration 2 allows to show that in some cases temporally resolved snapshot data is also available with the RT-PIV technique.

4.1 RT-PIV & planar 2D PIV - flow fields in a bidisperse packing (Configuration 1)

In the bidisperse packed bed the lowest layer of d=40mm spheres is investigated by RT-PIV and planar 2D PIV for Re_P = 200 to 700. In Fig. 5 upper left the raw particle field for Re_P =200 before the ray tracing correction is shown, while on the upper right the corrected particle field is presented. The rim region of the spheres does not contain any measurement signal in the raw images on the left, but strong reflections appear in the direction of the laser light sheet. Therefore, it is necessary to place masks at these regions for further processing (black circles in the corrected particle image). These correspond to the white regions in the vector fields shown in the lower line of Fig. 5.

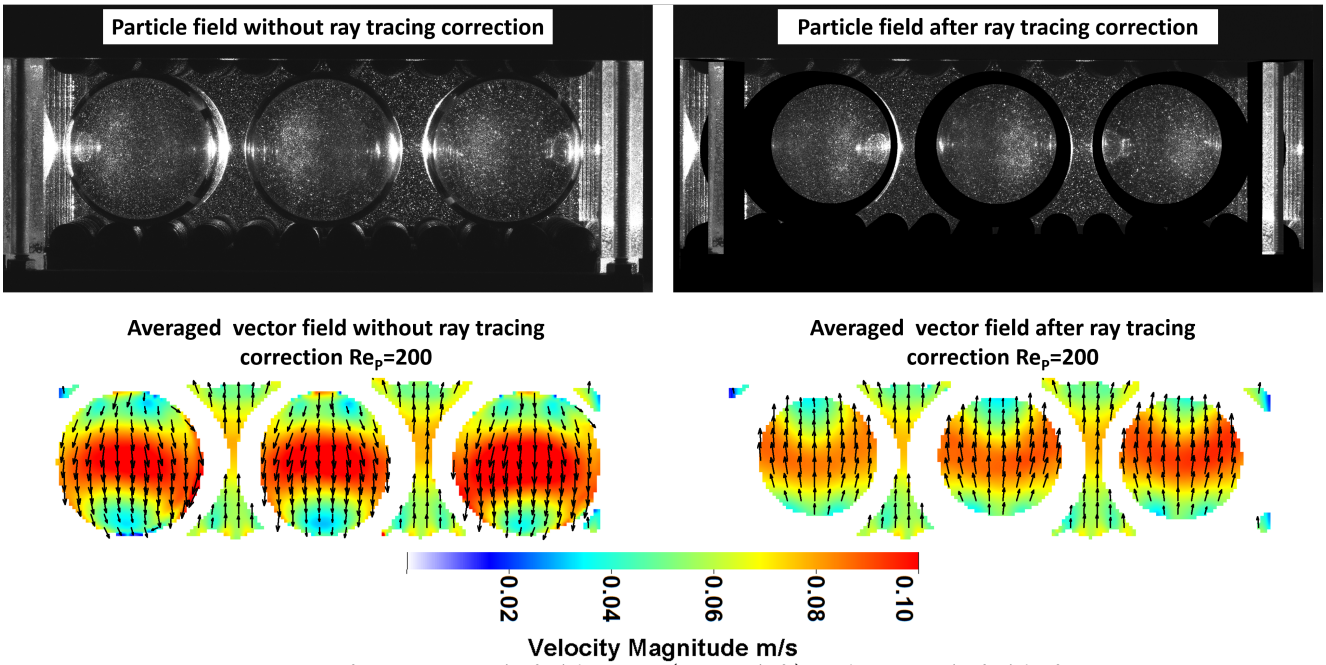

Figure 5 Comparison of a raw particle field image (upper left) and a particle field after ray tracing correction (upper right) and the averaged velocity vector fields based on the raw particle fields (lower left) and with distortion correction (lower right).

When evaluating directly the raw flow field, the flow is going upward in the regions with direct optical access between the spheres, but downwards in the optically obstructed area behind the spheres that is obviously not physical and due to the lens effect of the spheres (bottom left in Fig. 5). After ray tracing this effect is removed and the flow is moving correctly in the expected upward direction (bottom right in Fig. 5).

The pore behind a sphere has its smallest cross-sectional area at the sphere centre. Here the highest velocity appears. Below and above, the cross-sectional area increases again so that the velocity magnitude decreases. In the non-corrected vector field, the velocity magnitude appears to be higher, (maximum around 0.107m/s, bright red colour), while in the corrected vector field the velocity is around 0.088m/s (see orange/red colour). Besides the mirroring effect which explains the aforementioned inversed flow direction, the magnification caused by the glass spheres leads to a falsification of the velocity magnitude. The averaged vector fields show, with exception of the masked regions, a continuous flow field, which shows the success of the correction method.

In Fig. 6 an overview of the corrected velocity vector fields from RT-PIV for Re_P=200 to 700 is given on the left side and the vector fields of the easily accessible interstices by planar 2D PIV on the right side. Based on the RT-PIV data, it can be concluded that for all Re_P higher velocities appear at the height of the sphere centre. For the lowest Re_P=200 at the bottom of the layer no distinctive jets are visible which start to appear from Re_P=400. The velocity magnitude of these jets increases

with increasing Re_P. They are due to the interstices of the underlying sphere layers with smaller diameters.

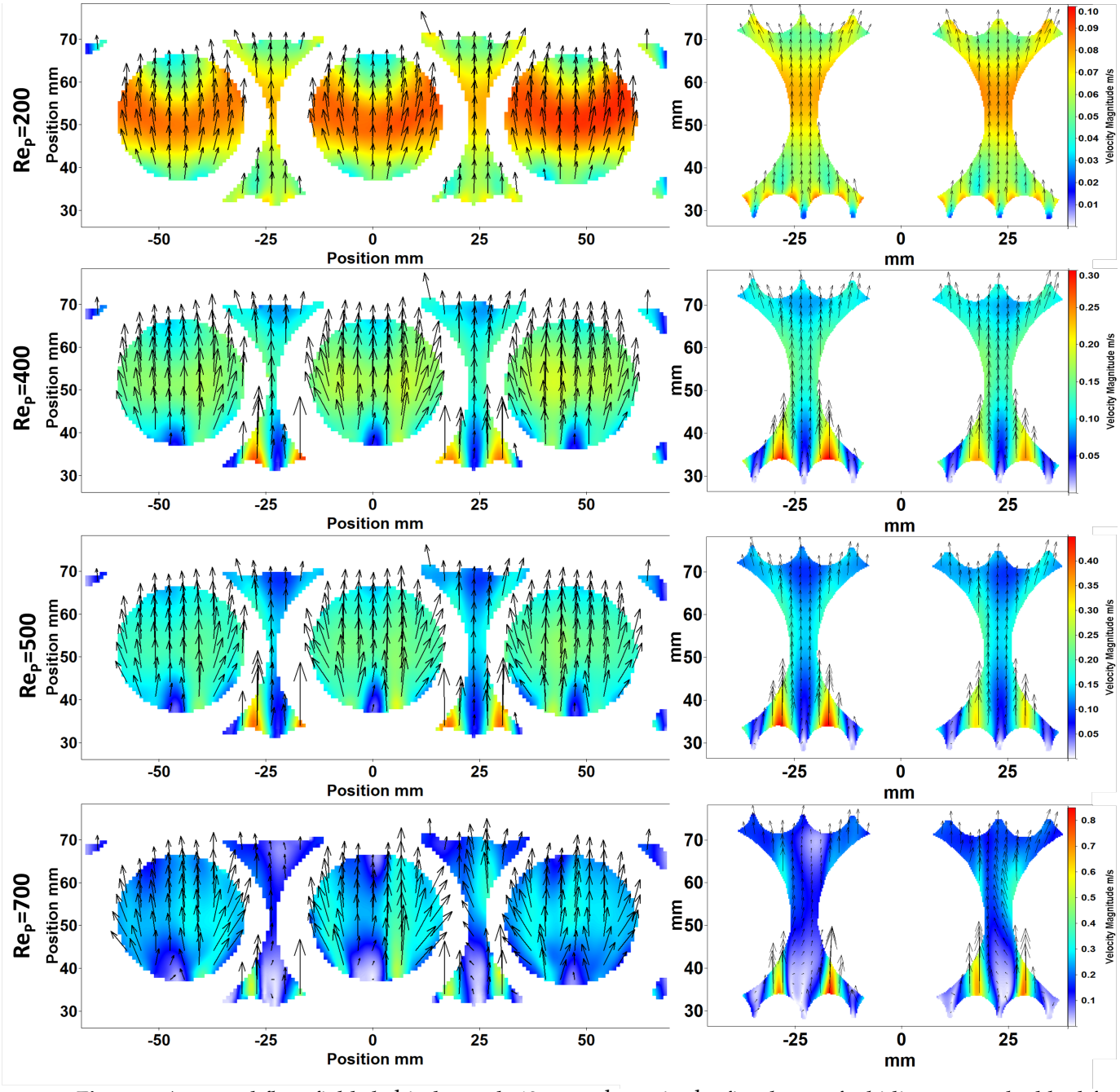

Figure 6 Averaged flow fields behind two d=40mm spheres in the first layer of a bidisperse packed bed for Re_P=200 to 700. The left column shows data obtained by RT-PIV allowing the view behind the packing material. In the right column data from planar 2D PIV of the easily accessible interstices is presented. While the colour plot represents the velocity magnitude, the overlying vectors represent the flow direction. Note that only every fourth vector is shown for the RT data and every 16th for the standard PIV data, as well as different colour scales are used for the different Re_P.

The flow fields obtained by planar 2D PIV in the optically easily accessible regions between the big spheres (Fig. 6 right) achieve high resolutions, coming without the bottlenecks of the

realisation of RT-PIV. A detailed discussion of these challenges will be given in Sec. 5. The flow fields of the two pores were obtained by two successive planar 2D PIV measurement series, which allowed for higher optical resolution, and are combined in Fig. 6 according to the geometry of the setup. By comparing the flow fields of both datasets it can be stated, that the same flow structure is obtained in both pores, especially for lower Re_P, while for higher Re_P some differences appear. For Re_P=700 the jet velocity in the left pore is higher (maximum jet velocity v_{max}= 0.565) compared to v_{max}= 0.771 m/s for the right pore.

When comparing the results of the flow fields in the pores obtained with the two different methods, some differences appear, that increase with Reynolds number. The resolution of the 2D PIV results is much higher, which is due to the much better raw image quality. Due to the increased DoF required for RT-PIV the image quality suffers more from diffusive light caused by reflections from the packing material or by the tracer particles themselves. For 2D planar PIV, frosted black spheres could be used instead of glass spheres which reduced much the appearance of reflections. The increased resolution, less reflections and different perspectives on the interstice for planar 2D PIV lead to a larger evaluation area closer to the rims of the spheres, so that the final vector field image appears lager. Nevertheless, the main flow features and velocity magnitudes are well captured by the RT-PIV method, which is the only one to allow for a look on the flow field "behind the spheres".

Nearly symmetrical flow fields are obtained with slight exceptions for the velocity magnitude in some cases. Therefore, the observation of one reactor half is sufficient for the further investigations. Since RT-PIV comes along with higher evaluation times as well as some experimental limitations, the measurement of the two remaining upper d=40mm sphere layers were carried out by planar 2D PIV and results are presented only for the left pore because of the symmetry assumption.

The velocity fields for these upper two layers are presented in Fig. 7, showing similar flow structures as in the first layer. Based on our previous work (Velten & Zähringer, 2023) this was expected due to the stabilization of the flow in the interior of the packing. Nevertheless, comparably lower velocities are present in the upper two layers compared to the first layer presented in Fig. 6. Before entering a d=40mm layer, the gas passes through five layers of d=10mm spheres in a body centred cubic arrangement. The results from S. Patil et al., (2024) show that for a bcc packing strong wall channelling appears. Since the first layer of the d=40mm system is closest to the reactor inlet, the flow is the most evenly distributed, since it only has passed five layers of d=10mm spheres before. In the second and third layer of d=40mm spheres wall channelling has increased since the flow has passed two more areas with five d=10mm layers and the velocities in the centre of the reactor decrease.

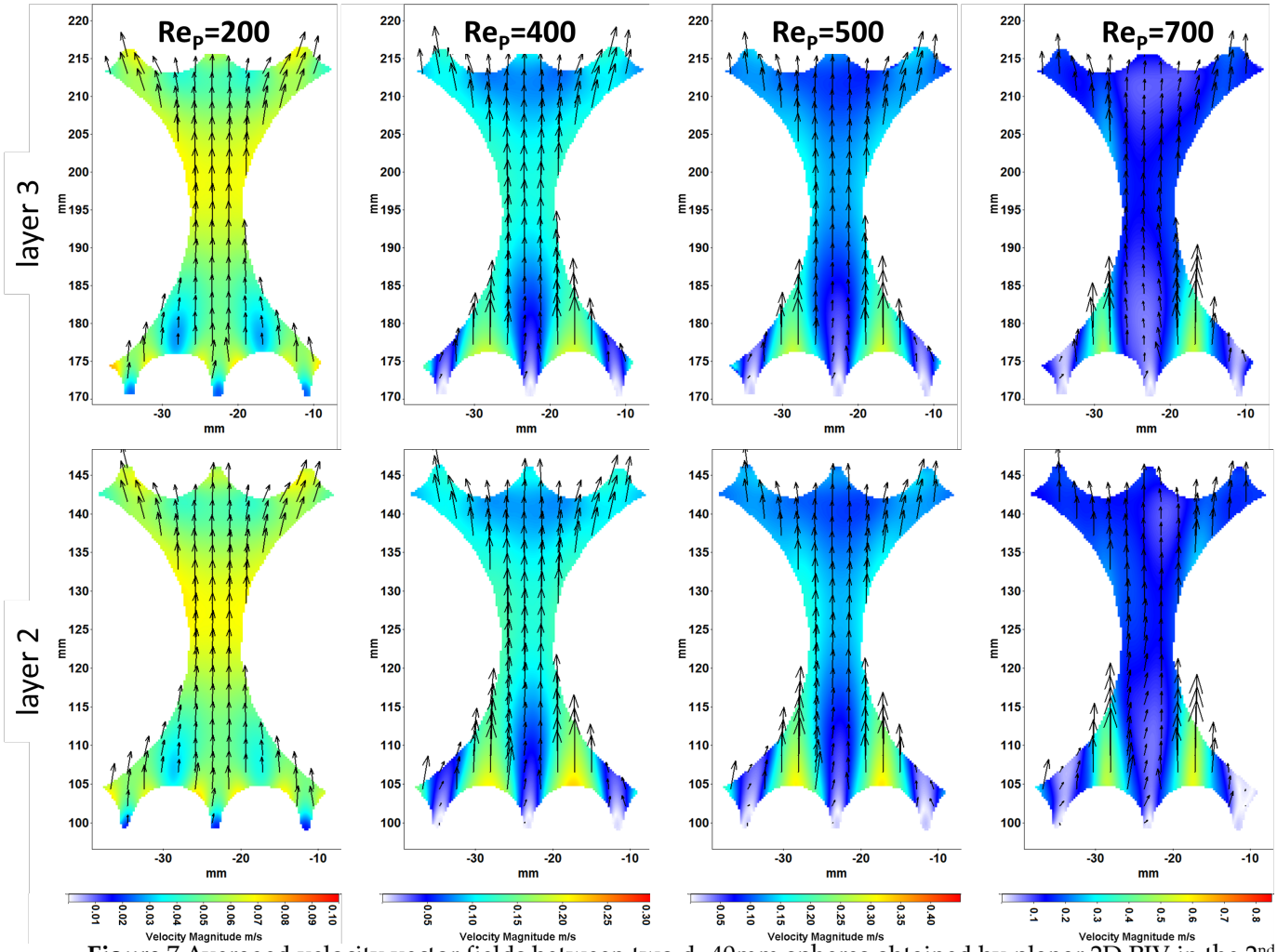

Figure 7 Averaged velocity vector fields between two d=40mm spheres obtained by planar 2D PIV in the 2nd and 3rd layer of big spheres in the bidisperse packed bed. The overlaying vector field represents the flow direction but only every 16th vector is shown. Note that different colour scales are used for the different Re_P=200 to 700.

4.3 RT-PIV - jet flow fields behind a central sphere (Configuration 2)

In Configuration 2 the jet flow around an individual sphere which is part of a 1.5-layer packed bed is investigated by RT-PIV. This configuration has no surrounding walls which leads to a reduction of reflexions due to less diffuse light in the system, thus improving the general image quality. Therefore, besides the averaged flow field also snapshot flow fields are better resolved.

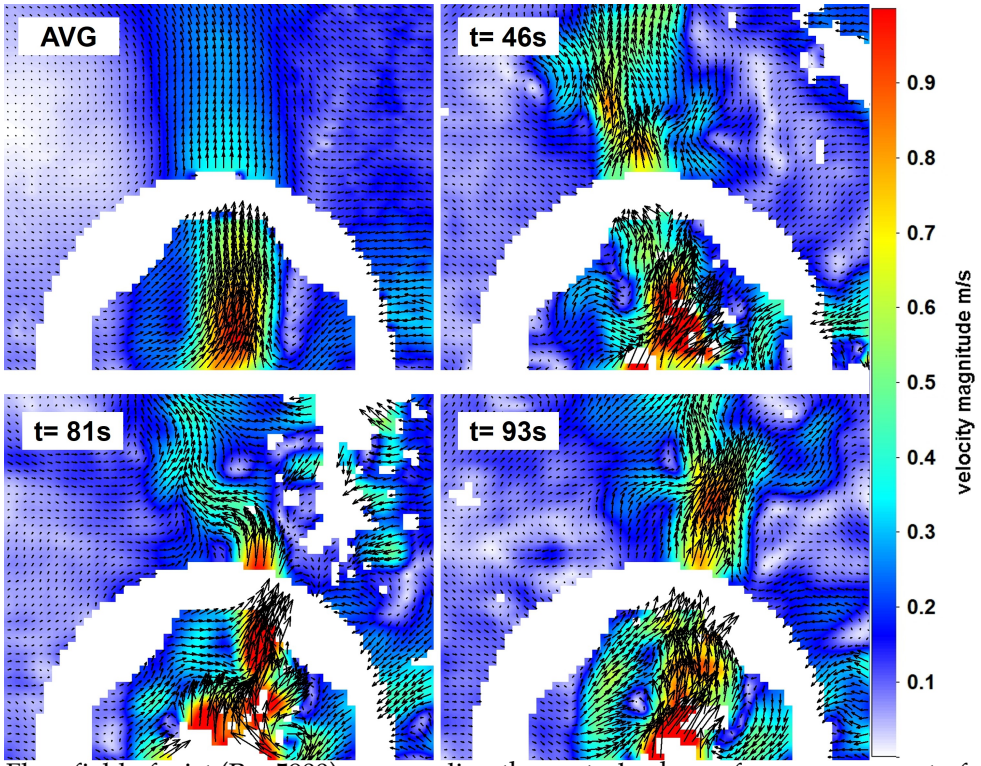

Figure 8 Flow field of a jet (Re=5900) surrounding the central sphere of an arrangement of d=40mm spheres in a bcc arrangement. In the upper left corner, the averaged flow field is shown while in the upper right and the lower line examples of snapshot flow fields are shown.

Figure 8 shows the averaged flow field (top left corner) and example snapshot flow fields (top right corner and lower line) for three different times (t= 46s; 81s and 93s). Since the jet is hitting the sphere at its bottom it can be expected that the flow is distributing around the sphere. The measurement position is situated behind this central sphere with a distance of approximately 23mm from the sphere centre, that means about 3mm from the sphere surface in the centre between the second and third sphere row. The averaged flow field demonstrates that the jet is deviated behind the sphere centre. This is the main characteristic of the flow since the velocity of the surroundings tends to zero. A more detailed insight to the flow characteristics is given by the snapshot data: the jet is fluctuating and causing different vortex structures in the surroundings. Note that only the jet is seeded with tracer particles, which leads to a non-homogeneous distribution of the tracer particles in the surroundings. This is the reason why the evaluation is only focussed on the very centred sphere and ignores the surrounding packing material.

This data proofs in principle the quantitative and qualitative applicability of RT-PIV for time resolved flow fields. But unfortunately, strong static reflections caused by the transparent spheres appeared in this measurement series which saturated the camera sensor. These reflections from the transparent packing material are one of the critical bottlenecks in the application of RT-PIV in packings and will be discussed in the following Sec. 5.

5. Challenges and Chances of RT-PIV

With a reliable distortion correction method, which in theory is provided by the ray tracing correction, nonintrusive optical measurements might be facilitated and this not only in the presented case of a solid-gas system.

Nevertheless, RT-PIV encounters several challenges which limit its application in transparent packings or reduce severely the quality of the results. Some of these issues where already discussed in our previous work (Velten et al., 2024).

First of all, the immense DoF which is required to capture images of the area behind the spheres and its free surroundings in focus is a severe experimental problem. Further, if working with bigger f-numbers because of the required DoF, the illumination might not be enough to generate a sufficient signal-to-noise ratio. On the other hand, reflections on the transparent packing material can saturate the camera sensor. Last but not least, the geometrical inaccuracies of the test rig due to real word manufacturing conditions cannot be reproduced by the light transport simulation. Most of these issues are interlinked, therefore by solving one, another might be reinforced. This dependency will be explained by two examples in the following.

We improved the accuracy of our geometry by 3D printing instead of an assembly of individual spheres. Thus, even if manufacturing tolerances remain (e.g. 0.3% for laser sintering of the PA12 material), a reproducible experimental arrangement is achieved. With an additional slit in the sphere layer below the measurement plane a calibration target can exactly be placed with connection to the geometry, so that the exact position of this geometry should be obtained. Since the final 3D-printed geometry differs slightly from the ideal CAD-file, differences to the ideal geometry used for the simulation will exist. Unfortunately, the light transport simulation is highly sensitive to a shift in the sphere positon and the refractive index of the transparent material. Therefore, we implemented a numerical optimization routine for these two parameters, as explained in Sec. 3. By varying the refractive index and the sphere position with respect to the camera different optimal solutions can be obtained, from which the most physical one has to be chosen. This process requires computational times much longer than standard PIV evaluations.

The second example is that of the DoF which needs to be around 15cm for our presented setups since the spheres act as lenses and shift the focus of the measurement plane in the direction of the camera. To remediate this problem, we used a camera lens with a small angle of view which allows to place the camera further away from the setup. Nevertheless, a f-number of around 12 is still needed that is far away from those recommended for PIV, and still not delivering an optimal signal-to-noise ratio. If then the laser power is increased to compensate, the reflections on the

transparent packing material are strengthened. These reflections are caused by the light sheet hitting the geometry and the surrounding acrylic box, or by reflections of the Mie scattering of the tracer particles on the glass spheres. This additional diffusive light is captured by the camera due to the immense DoF and decreases the signal-to-noise ratio. The easiest way to avoid these issues would be the use of fluorescent tracer particles but the fluorescence signal is very weak, compared to Mie scattering, and therefore no alternative in the present high f-number arrangement. Therefore, only post processing of the raw PIV images like filtering the background and static reflections as well as intensity normalisation can slightly increase the image quality. This treatment is sufficient to obtain averaged results if enough images are recorded.

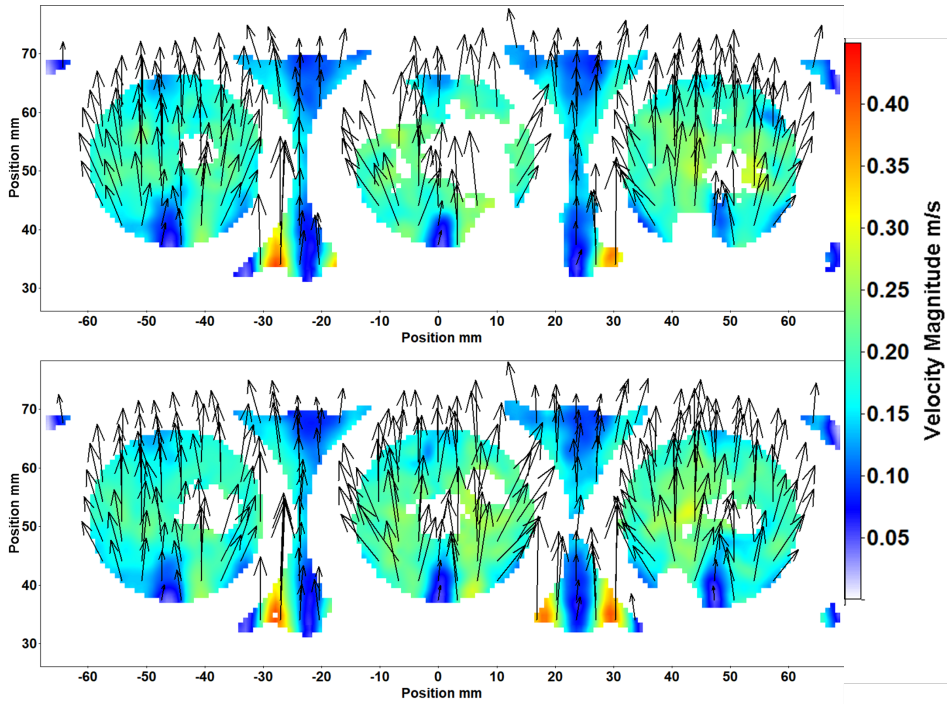

Figure 9 Two snapshot velocity fields for Re_P=500 in the first layer of d=40mm spheres of Configuration 1. The vector fields are incomplete due to bad correlation values in some regions of the image, where the signal-to-noise ratio is low according to the issues discussed in the text

For snapshot data, especially at higher Re_P when three-dimensionality of the flow is increased, the aforementioned poor image quality leads to large regions where no sufficient correlation values can be achieved. Therefore, the evaluation of snapshot data or turbulence quantities becomes difficult. Fig. 9 shows such snapshot velocity fields for Configuration 1 at Re_P=500. The white regions where vectors are missing correspond to masks applied during the vector post processing and the aforementioned bad correlation values, where no reliable velocity data can be obtained due to a bad signal-to-noise ratio.

This discussion shows that the application of RT-PIV is experimentally and numerically complex. The data presented in this work underlines the possibility to obtain data by RT-PIV in the inner of a transparent packed bed, especially for averaged flow data. Nevertheless, the complexity of the method and the discussed drawbacks would exclude for example tomographic or stereo PIV in setups like those examined in this study. In transparent systems causing minor distortions than the here presented spheres or if smaller differences in the refractive indices apply, the RT correction method might deliver a good tool for distortion correction, if the exact geometry of the setup is known for the simulations.

6. Conclusions

Two different configurations where investigated to obtain flow fields inside packed beds by RT-PIV. Configuration 1 represents a packed bed of d=10 and d=40mm spherical particles in bcc arrangement. The flow for Re_P in a range from 200 to 700 was investigated by RT-PIV and compared to planar 2D PIV measurements. When using transparent packing material to generate the optical access, distortions are introduced to the raw measurement images which are successfully corrected by a ray tracing based correction. This method relies on a light transport simulation through the geometry of the experimental test rig to obtain the knowledge of distorted and corrected pixel positions.
The flow fields corrected by RT-PIV are in good agreement with those obtained by planar 2D PIV in the easily accessible interstices but with way lower resolution and some minor differences in the velocity magnitude. The flow inside the bed is steady and does not significantly change from layer to layer (concerning the d=40mm sphere layers). The influence of the reduced cross-section due to the d=40mm particles can be seen by an increased velocity magnitude, as well as the jets produced by the underlying layers of d=10mm spheres. The magnitude of the jets increases with Reynolds number.
In Configuration 2 a jet at Re=5900 surrounding a glass sphere of d=40mm in a bcc arrangement of 1.5 layers was investigated. By applying RT-PIV, temporally resolved snapshot data of the velocity field behind the sphere was obtained. The limitations and drawbacks of RT-PIV mainly related to a reduced signal-to-noise ratio of the raw images were also discussed.

Acknowledgments

Funded by the Deutsche Forschungsgemeinschaft (DFG, German Research Foundation) – Project-ID 422037413 – SFB/TR 287, Project A1.
The authors would like to acknowledge Kerstin Hüls for her help in performing the experiments.

References

Kováts, P., Thévenin, D., & Zähringer, K. (2015, September). Experimental investigation of flow fields within cavities of coarse packed bed. Fachtagung "Lasermethoden in der Strömungsmesstechnik", 54-1-7.

Martins, F., Da Carvalho Silva, C., Lessig, C., & Zähringer, K. (2018a). Ray-Tracing Based Image Correction of Optical Distortion for PIV Measurements in Packed Beds. Journal of Advanced Optics and Photonics, 1(2), 71–94. https://doi.org/10.32604/jaop.2018.03870

Martins, F., Da Carvalho Silva, C., Lessig, C., & Zähringer, K. (2018b). Ray-Tracing Based Image Correction of Optical Distortions Caused by Transparent Spheres for Application in PIV. 19th International Symposium on the Application of Laser and Imaging Techniques to Fluid Mechanics (16-19 July, 2018 Lisbon), pp. 2.8.2.

Nguyen, T., Muyshondt, R., Hassan, Y. A., & Anand, N. K. (2019). Experimental investigation of cross flow mixing in a randomly packed bed and streamwise vortex characteristics using particle image velocimetry and proper orthogonal decomposition analysis. Physics of Fluids, 31(2), 25101. https://doi.org/10.1063/1.5079303

Patil, S., Gorges, C., Lòpez Bonilla, J., Stelter, M., Beyrau, F., & van Wachem, B. (2024). Experimental and numerical investigation to elucidate the fluid flow through packed beds with structured particle packings. Particuology, 89, 218–237. https://doi.org/10.1016/j.partic.2023.11.002

Patil, V. A., & Liburdy, J. A. (2013). Flow characterization using PIV measurements in a low aspect ratio randomly packed porous bed. Experiments in Fluids, 54(4). https://doi.org/10.1007/s00348-013-1497-3

Velten, C., Ebert, M., Lessig, C., & Zähringer, K. (2024). Ray tracing particle image velocimetry – Challenges in the application to a packed bed. Particuology, 84, 194–208. https://doi.org/10.1016/j.partic.2023.06.003

Velten, C., & Zähringer, K. (2023). Flow Field Characterisation of Gaseous Flow in a Packed Bed by Particle Image Velocimetry. Transport in Porous Media, 150(2), 307–326. https://doi.org/10.1007/s11242-023-02010-7